

# A New Nuclear Model for Neutrinoless $\beta\beta$ -Decay and Double Charge-Exchange Resonances

C. De Conti<sup>1</sup>, V. dos S. Ferreira<sup>2</sup>, A.R. Samana<sup>2</sup>, C.A. Barbero<sup>3</sup>, and F. Krmpotić<sup>3</sup>

<sup>1</sup>*Campus Experimental de Rosana, Universidade Estadual Paulista, CEP 19274-000, Rosana, SP, Brazil*

<sup>2</sup>*Departamento de Ciências Exatas e Tecnológicas,*

*Universidade Estadual de Santa Cruz, CEP 45662-000 Ilhéus, Bahia-BA, Brazil, and*

<sup>3</sup>*Instituto de Física La Plata, CONICET, Universidad Nacional de La Plata, CP 1900 La Plata, Argentina.*

We have recently developed a nuclear model, specially designed to describe double charge exchange (DCE) processes, which is a natural extension of the  $pn$ -QRPA model for  $\beta$ -decay to  $\beta\beta$ -decay. Ergo, this model, in addition to including the pairing correlations and having the same number of free parameters, brings into play the  $ppnn$ -quasiparticle excitations and the Pauli Principle, which are essential ingredients to correctly account for the nuclear matrix elements (NMEs) for  $\beta\beta$ -decays and nuclear reactions to all  $0^+$  and  $2^+$  final states, including resonances, and not just to the ground state as in  $pn$ -QRPA. In addition, it allows us to evaluate the  $Q_{\beta\beta}$ -values, and the excitation energies in final nucleus, and to work with a single-particle space large enough for the DCE sum rules to be satisfied. So far it has been applied to the  $2\nu\beta\beta$ -decay, and here we extend it to the  $0\nu\beta\beta$ -decay. The model that comes closest in terms of its advantages is the shell model. We describe here the DCE observables in: i)  $^{76}\text{Se}$ , which have been recently measured in the GERDA and MAJORANA Experiments, and ii)  $^{124}\text{Te}$ , for which has been reported recently the first direct observation of  $2\nu$  double electron capture with the XENON1T Dark Matter detector. A good agreement with the data is obtained for both the ground state and the excited states. We have found that the reaction and  $0\nu\beta\beta$ -decay NMEs are of the same order of magnitude even in the region of giant resonances.

PACS numbers: 14.60.Lm, 21.60.-n, 23.40.Bw, 23.40.-s

## I. INTRODUCTION

If the driving mechanism of the  $0\nu\beta\beta$ -decay is through the exchange of a left-handed light neutrino of Majorana type, which is forbidden in the Standard Model, its detection will allow us to find the effective mass of the neutrino  $\langle m_\nu \rangle$ , provided we know the nuclear matrix element (NME)  $M^{0\nu}$ , since the decay amplitude is proportional to  $|\langle m_\nu \rangle M^{0\nu}|^2$ .

These NMEs are calculated using different nuclear models, and there are no experimental data or model-independent sum rule to corroborate their calculated values. As a consequence, a large scatter in the results (up to factors of three) has emerged.

Strictly speaking, despite the enormous efforts invested in these calculations, we are still not entirely sure of the order of magnitude of the NMEs  $M^{0\nu}$  [1]. We also do not know what is the total transition intensity of the  $0\nu\beta\beta$ -decay, and what is the proportion of it that ends in the ground state. We will try to give an answer to these questions.

We know this only for the double Gamow-Teller (DGT) operator from the work of Auerbach et al. [2–5], but not for  $M^{0\nu}$ .

In recent years much attention is being paid to  $\beta\beta$ -decays to excited states in final nuclei, and there are several large underground experiments operating for detection of  $\langle m_\nu \rangle$ , such as the GERDA and MAJORANA searches in  $^{76}\text{Ge}$  [6, 7].

On the other hand, the NUMEN heavy ion multidecay, designed for a complementary approach to  $0\nu\beta\beta$  NMEs, is currently taking data [8–12]. Theoretical com-

parisons have been made [13–16] between the  $0\nu\beta\beta$  NME and the DGT transition to the to the ground state of the final nucleus, where a very small portion of the total strength is found.

In addition to evaluating the  $\beta\beta^-$ -decays of  $^{76}\text{Ge}$ , we also discuss the  $\beta\beta^+$ -decays of  $^{124}\text{Xe}$ , where has been done the first direct observation of the  $2\nu$  double electron capture ( $2\nu ee$ ) for the ground state in  $^{124}\text{Te}$ , with the half-life  $\tau_{2\nu}^{ee}(0_1^+) = (1.8 \pm 0.6) \times 10^{22}$  y [17], which is the longest half-life ever measured directly, about one trillion times the age of the Universe. More recently, by a XMASS experiment [18] has been imposed the constraint on this half-life  $\tau_{2\nu}^{ee}(0_1^+) > 2.1 \times 10^{22}$  y at 90% confidence level, which is consistent with above measurement.

The single charge-exchange (SCE) operators  $\mathcal{O}_0^\mp = \tau^\mp$ , and  $\mathcal{O}_1^\mp = \tau^\mp \sigma$ , play a fundamental role in  $\beta^\mp$ -decays:  $(A, Z) \rightarrow (A, Z \pm 1)$ . In the same way, the double charge-exchange (DCE) operators  $\mathcal{D}_{J\mathcal{J}}^\mp = [\mathcal{O}_J^\mp \times \mathcal{O}_{\mathcal{J}}^\mp]_{\mathcal{J}}$ , with  $J = 0, 1$ , and  $\mathcal{J} = 0, 2$ , are essential for the  $\beta\beta^\mp$ -decays:  $(A, Z) \rightarrow (A, Z \pm 2)$ , and closely related to the  $0\nu$  and  $2\nu$  NMEs. In turn, the operators  $\mathcal{O}_J$ , and  $\mathcal{D}_{J\mathcal{J}}^\mp$  are related to the corresponding SCE, and DCE reaction processes, and their giant resonances.

The nuclear models are employed to evaluate the total SCE strengths

$$S_J^{\{\mp 1\}} \equiv \sum_i |\langle J_i | \mathcal{O}_J^\mp | 0^+ \rangle|^2 \equiv \sum_i s_J^{\{\mp 1\}}(J_i), \quad (1)$$

going from the initial ground state  $|0^+\rangle$  to intermediate

states  $|J_i^+\rangle$ , as well as the total DCE strengths

$$S_{J\mathcal{J}}^{\{\mp 2\}} = \sum_f |\langle \mathcal{J}_f | \mathcal{D}_{J\mathcal{J}}^{\mp} | 0^+ \rangle|^2 \equiv \sum_f s_{J\mathcal{J}}^{\{\mp 2\}}(\mathcal{J}_f), \quad (2)$$

going from  $|0^+\rangle$  to final states  $|\mathcal{J}_f\rangle$ .

When both  $|J_i\rangle$  and  $|\mathcal{J}_f\rangle$  are complete sets of states that can be reached by operating with  $\mathcal{O}_J^\pm$ , and  $\mathcal{D}_{J\mathcal{J}}^\pm$  on  $|0^+\rangle$ , the strength differences

$$\begin{aligned} S_J^{\{1\}} &= S_J^{\{-1\}} - S_J^{\{+1\}}, \\ S_{J\mathcal{J}}^{\{2\}} &= S_{J\mathcal{J}}^{\{-2\}} - S_{J\mathcal{J}}^{\{+2\}}, \end{aligned} \quad (3)$$

obey the SCE Ikeda's sum rules [19]

$$S_J^{\{1\}} = N - Z, \quad (4)$$

and the DCE sum rules [2, 20, 21]

$$S_{00}^{\{2\}} = 2(N - Z)(N - Z - 1), \quad (5)$$

$$S_{10}^{\{2\}} = 2(N - Z) \left( N - Z + 1 + 2S_1^{\{-1\}} \right) - \frac{2}{3}C,$$

$$S_{12}^{\{2\}} = 10(N - Z) \left( N - Z - 2 + 2S_1^{\{-1\}} \right) + \frac{5}{3}C,$$

where  $C$  is a relatively small positive quantity, given by [21, Eq. (4)]. Since the terms proportional to  $C$  are not considered in (5), the following inequalities arise:

$$S_{10}^{\{2\}} \geq S_{10}^{\{2\}}, \quad S_{12}^{\{2\}} \leq S_{12}^{\{2\}}. \quad (6)$$

It is desirable that any nuclear model used to calculate the DCE processes satisfy the sum rules (5) for the total strengths  $S_{J\mathcal{J}}^{\{\mp 2\}}$ . We can now evaluate the fractions of strengths going to the individual states as

$$\begin{aligned} R^{\{\mp 1\}}(J_i) &= s_J^{\{\mp 1\}}(J_i) / S_J^{\{\mp 1\}}, \\ R_{J\mathcal{J}}^{\{\mp 2\}}(\mathcal{J}_f) &= s_{J\mathcal{J}}^{\{\mp 2\}}(\mathcal{J}_f) / S_{J\mathcal{J}}^{\{\mp 2\}}, \end{aligned} \quad (7)$$

calibrating in this way the NMEs of the operators  $\mathcal{O}_J$  and  $\mathcal{D}_{J\mathcal{J}}$ . Later the same will be done with the  $0\nu\beta\beta$  NME, which will allow us to determine their order of magnitude.

The  $0\nu\beta\beta$  NMEs for the final  $0^+$  and  $2^+$  states are completely different from each other, since they are spawned from different parts of the vector (V), and axial-vector (A) weak-hadronic-currents  $J^\mu = (\rho, \mathbf{j})$ ; see, for instance [22, Eqs.(7), (8)]. In fact, while the first comes from  $\rho_V$ , and  $\mathbf{j}_A$ , which are akin to  $\mathcal{D}_{00}$ , and  $\mathcal{D}_{10}$ , respectively, the second comes from the velocity dependent parts of  $\mathbf{j}_V$ , and  $\mathbf{j}_A$ , that do not resemble  $\mathcal{D}_{12}$ ; see, [24, Eqs.(5), (6)]. Because of this,  $0\nu\beta\beta$ -decays to final states  $2^+$  are not considered here.

In the case of  $0^+$  final states, pseudoscalar (P), and weak magnetism (M) induced currents also contribute to

the  $0\nu\beta\beta$ -decay, and the corresponding NME,  $M^{0\nu^\mp}(0_f^+)$ , is usually presented as a sum of F, GT, and Tensor (T) parts (see, for example,[25, Eq. (3)]). The term F arises only from the V weak current, but the GT and T terms contain mixtures of A, M, and P currents (see Refs. [22, 23, 26, 38]). We prefer to highlight the individual contributions of the weak currents, and write

$$M^{0\nu^\mp}(0_f^+) = \sum_X M_X^{0\nu^\mp}(0_f^+), \quad (8)$$

where  $X = V, A, M, P$ . The weak coupling constants  $g_V, g_A, f_M = (g_M + g_V)/(2M_N)$ , and  $g'_P = g_P/(2M_N)$  are incorporated within  $M_X^{0\nu^\mp}(0_f^+)$ .

The DCE NMEs

$$M_{J\mathcal{J}}^{\mp}(\mathcal{J}_f) \equiv \langle \mathcal{J}_f | \mathcal{D}_{J\mathcal{J}}^{\mp} | 0^+ \rangle, \quad (9)$$

where  $M_{00}^{\mp}$  is double Fermi (DF), and  $M_{10}^{\mp}$  and  $M_{12}^{\mp}$  are, respectively, monopole and quadrupole double Gamow-Teller (DGT) matrix elements. We will call them generically DCE Reaction (DCER) NMEs, since they can be observed experimentally only through nuclear reactions, as well as to differentiate them from the  $\beta\beta$  NMEs.

We note here that the designation DGT NME is used in the literature for the ground state NME  $M_{10}^-(0_1^+)$ . [1–5, 13–16].

On the other hand, the value of  $M^{0\nu^-}(0_1^+)$  is usually inferred from heavy-ion reaction data at low momentum transfer<sup>1</sup>, using  $M_{10}$  and  $M_{00}$  for  $M_A^{0\nu}$  and  $M_V^{0\nu}$ , respectively, even though these NMEs differ from each other in several aspects, as will be shown later on.

In the present work we will go a few steps further than what has been done in Refs. [13–16], comparing the NMEs in all final states that are reached by the  $\beta\beta$ -decay, and not only in the ground state, and extending this study along the full strength distributions for the  $0\nu\beta\beta$ -decays and DCERs.

For this purpose, we introduce two new quantities:

1) The total  $0\nu\beta\beta^\mp$  strengths  $S^{0\nu^\mp}$ , and their energy distributions  $s^{0\nu^\mp}(0_f^+)$ , define as

$$S^{0\nu^\mp} = \sum_f |M^{0\nu^\mp}(0_f^+)|^2 \equiv \sum_f s^{0\nu^\mp}(0_f^+), \quad (10)$$

as well as the ratios

$$R^{0\nu^\mp}(0_f^+) = s^{0\nu^\mp}(0_f^+) / S^{0\nu^\mp}; \quad (11)$$

and

2) The folded transition densities in  $(A, Z \pm 2)$  nuclei

$$\mathcal{S}_{J\mathcal{J}}^{\{\mp 2\}}(\mathcal{E}) = \frac{\Delta}{\pi} \sum_f \frac{s_{J\mathcal{J}}^{\{\mp 2\}}(\mathcal{J}_f)}{(\mathcal{E} - \mathcal{E}_f)^2 + \Delta^2}, \quad (12)$$

<sup>1</sup> (See for example [71, Eq. (16)]).

as a function of excitation energies

$$\mathcal{E}_f = E_{0_f^+}^{\{\mp 2\}} - E_{0_1^+}^{\{\mp 2\}}, \quad (13)$$

of the final states  $|0_f^+\rangle$ , with the energy interval  $\Delta = 1$  MeV.

We will calculate (10), (11), and (12) as well for  $S_V^{0\nu\mp}$ ,  $S_{A_{1+}}^{0\nu\mp}$ ,  $S_A^{0\nu\mp}$ , and  $S^{0\nu\mp}$ , and define  $\mathcal{S}_V(\mathcal{E})$ , and  $\mathcal{S}_A(\mathcal{E})$  the same way as  $\mathcal{S}_{JJ}^{\{\mp 2\}}(\mathcal{E})$ . We will not do so for the  $2\nu\beta\beta$ -decay since in this case the transition density  $\mathcal{S}(\mathcal{E})$  fluctuates greatly in energy.

The reaction folded strength densities meet the relationship

$$\int d\mathcal{E} \mathcal{S}_{JJ}^{\{\mp 2\}}(\mathcal{E}) = S_{JJ}^{\{\mp 2\}}, \quad (14)$$

and the same for  $\mathcal{S}_V(\mathcal{E})$ , and  $\mathcal{S}_A(\mathcal{E})$ .

Note that, due to the neutron excess, in the medium and heavy nuclei, it occurs that

$$S_{JJ}^{\{-2\}} \gg S_{JJ}^{\{+2\}}, \text{ and } S_{V,A}^{0\nu-} \gg S_{V,A}^{0\nu+}. \quad (15)$$

## II. FORMALISM

### A. Nuclear Matrix Elements, Half Lives, and Q-values

Independently of the nuclear model that is used, the  $2\nu\beta\beta$  NMEs can be expressed as

$$M_J^{2\nu\mp}(\mathcal{J}_f) = \frac{-g_J^2}{\sqrt{\mathcal{J}+1}} \sum_i \frac{\langle \mathcal{J}_f | | \mathcal{D}_{J_i \mathcal{J}}^{\mp} | | 0^+ \rangle}{\left( \mathcal{D}_{J_i, \mathcal{J}_f}^{2\nu\mp} \right)^{\mathcal{J}+1}}, \quad (16)$$

where  $J = 0$  and  $J = 1$  stand, respectively, to F and GT transitions, and  $g_0 \equiv g_V$  and  $g_1 \equiv g_A$  are the corresponding weak coupling constants.  $\langle \mathcal{J}_f | | \mathcal{D}_{J_i \mathcal{J}}^{\mp} | | 0^+ \rangle$  is a short notation for  $\langle \mathcal{J}_f^+ | | \mathcal{O}_J^{\pm} | | J_i^+ \rangle \langle J_i^+ | | \mathcal{O}_J^{\pm} | | 0^+ \rangle$ . The summation goes over all intermediate virtual states  $|J_i\rangle$  in the nuclei  $(A, Z \mp 1)$ . Moreover,

$$\begin{aligned} \langle \mathcal{J}_f | | \mathcal{D}_{J_i \mathcal{J}}^{\mp} | | 0^+ \rangle &= \sum_{p_1 n_1 p_2 n_2} \varrho^{\mp}(p_1 n_1 p_2 n_2; J_i, \mathcal{J}_f) \\ &\times W_{0JJ}(p_1 n_1) W_{0JJ}(p_2 n_2), \end{aligned} \quad (17)$$

with

$$\begin{aligned} \varrho^{\mp}(p_1 n_1 p_2 n_2; J_i, \mathcal{J}_f^+) &= \hat{J}^{-2} \langle \mathcal{J}_f^+ | | (c_{p_2}^{\dagger} c_{n_2})_J | | J_i \rangle, \\ &\times \langle J_i | | (c_{p_1}^{\dagger} c_{n_1})_J | | 0^+ \rangle \end{aligned} \quad (18)$$

being the two-body density matrix, where  $c_p^{\dagger}$  and  $c_{\bar{n}}$  are, respectively, proton creation and neutron annihilation

operators. The angular parts are given by <sup>2</sup>:

$$W_{LSJ}(pn) = \sqrt{2} \hat{S} \hat{J} \hat{L} \hat{L}_n \hat{J}_n \hat{J}_p (l_n L | l_p) \begin{Bmatrix} l_p & \frac{1}{2} & j_p \\ L & S & J \\ l_n & \frac{1}{2} & j_n \end{Bmatrix}, \quad (19)$$

where  $(l_n L | l_p) \equiv (l_n 0 L 0 | l_p 0)$ . Finally, the energy denominator is

$$\begin{aligned} \mathcal{D}_{J_i \mathcal{J}_f}^{\mp} &= E_{J_i}^{\{\mp 1\}} - \frac{E_{0_+}^{\{0\}} + E_{\mathcal{J}_f}^{\{\mp 2\}}}{2} \\ &= E_{J_i}^{\{\mp 1\}} - E_{0_+}^{\{0\}} + \frac{E_{0_+}^{\{0\}} - E_{\mathcal{J}_f}^{\{\mp 2\}}}{2}, \end{aligned} \quad (20)$$

where  $E_{0_+}^{\{0\}}$ ,  $E_{J_i}^{\{\mp 1\}}$ , and  $E_{\mathcal{J}_f}^{\{\mp 2\}}$  are the energies of: (i) the ground state of the decaying nucleus  $(A, Z)$ , (ii) the  $J_i^+$  state in the intermediate nucleus  $(A, Z \pm 1)$ , and (iii) the  $\mathcal{J}_f^+$  state in the final nucleus  $(A, Z \pm 2)$ ; respectively.

The  $0\nu\beta\beta$  NMEs can always be put in the form (8), with Finite Nucleon Size effects introduced through the usual dipole form factors

$$\begin{aligned} g_V &\rightarrow g_V(k^2) \equiv g_V \Lambda_V^4 (\Lambda_V^2 + k^2)^{-2}, \\ g_A &\rightarrow g_A(k^2) \equiv g_A \Lambda_A^4 (\Lambda_A^2 + k^2)^{-2}, \\ f_M &\rightarrow f_M(k^2) \equiv f_M \Lambda_V^4 (\Lambda_V^2 + k^2)^{-2}, \\ g'_P &\rightarrow g'_P(k^2) \equiv g'_P \Lambda_A^4 (\Lambda_A^2 + k^2)^{-2}, \end{aligned} \quad (21)$$

where  $\Lambda_V = 0.85$  GeV, and  $\Lambda_A = 1.086$  GeV are the cut-off parameters as found in [37, 42, 81]. The Short Range Correlations are included in the way indicated in [26, Eqs. (2.29)-(2.31)].

The weak coupling constants are fixed as follows:  $g_V = 1$ , and  $g_M = 3.7$  from Conservation of Vector Current,  $g_A = 1.27$  from the experimental data [44], and  $g_P = 2M_N g_A / (q^2 + m_\pi^2)$  from the assumption of Partially Conserved Axial Current [45].

Like the NMEs of  $2\nu\beta\beta$ , the  $M_X^0(0_f)$  in (8) can be expressed by the density matrix  $\varrho^{\mp}$ , as follows

$$\begin{aligned} M_X^{0\nu\mp}(0_f^+) &= \sum_{J_i} \sum_{p_1 p_2 n_1 n_2} \varrho^{\mp}(p_1 n_1 p_2 n_2; J_i^{\mp} 0_f) \\ &\times m_X^{0\nu}(p_1 n_1 p_2 n_2; J, \mathcal{D}_{J_i, 0_f}), \end{aligned} \quad (22)$$

where  $m_X^{0\nu}(p_1 n_1 p_2 n_2; \mathcal{D}_{J_i, 0_f})$  are the single particle  $0\nu\beta\beta$  NMEs, which do not depend of nuclear models.

Because the  $0\nu\beta\beta$  NMEs depend only very weakly on the energy denominators  $\mathcal{D}_{J_i^{\mp}, 0_f^+}$ , calculations are usually performed in the Closure Approximation (CA), where these are approximated by a constant value  $\mathcal{D}$  of the order of 10 MeV [25]. This greatly simplifies the numerical

<sup>2</sup> We use here the angular momentum coupling scheme  $|(l, l, j)\rangle$ .

calculations, and it will be done here. Eq. (22) becomes

$$M_X^{0\nu^\mp}(0_f) = \sum_J \sum_{p_1 p_2 n_1 n_2} \bar{\varrho}^\mp(p_1 n_1 p_2 n_2; J, 0_f) \times m_X^{0\nu}(p_1 n_1 p_2 n_2; J, \mathcal{D}), \quad (23)$$

where

$$\bar{\varrho}^\mp(p_1 n_1 p_2 n_2; J, 0_f) = \sum_i \varrho^\mp(p_1 n_1 p_2 n_2; J_i 0_f). \quad (24)$$

The single particle  $0\nu\beta\beta$  NMEs can be derived from [26, Eqs. (20)], and they are:

$$m_V^{0\nu}(p_1 p_2 n_1 n_2; J, \mathcal{D}) = W_{J0J}(p_1 n_1) W_{J0J}(p_2 n_2) \times \mathcal{R}_{JJ}^V(p_1 n_1 p_2 n_2; \mathcal{D}), \quad (25)$$

$$m_A^{0\nu}(p_1 p_2 n_1 n_2; J, \mathcal{D}) = \sum_L W_{L1J}(p_1 n_1) W_{L1J}(p_2 n_2) \times (-)^{L+1} \mathcal{R}_{LL}^A(p_1 n_1 p_2 n_2; \mathcal{D}), \quad (26)$$

$$m_P^{0\nu}(p_1 p_2 n_1 n_2; J, \mathcal{D}) = - \sum_{LL'l} (-)^{J+(L+L')/2} \hat{L} \hat{L}' (LL'l|l) \times (11|l) W_{L1J}(p_1 n_1) W_{L'1J}(p_2 n_2) \times \left\{ \begin{matrix} L & L' & l \\ 1 & 1 & J \end{matrix} \right\} \mathcal{R}_{LL'}^P(p_1 n_1 p_2 n_2; \mathcal{D}), \quad (27)$$

and

$$m_M^{0\nu}(p_1 p_2 n_1 n_2; J, \mathcal{D}) = - \sum_{LL'l} (-)^{J+(L+L')/2} \hat{L} \hat{L}' (LL'l|l) \times (11|l) W_{L1J}(p_1 n_1) W_{L'1J}(p_2 n_2) \left[ 2 - \frac{l(l+1)}{2} \right] \times \left\{ \begin{matrix} L & L' & l \\ 1 & 1 & J \end{matrix} \right\} \mathcal{R}_{LL'}^M(p_1 n_1 p_2 n_2; \mathcal{D}). \quad (28)$$

We note that  $m_V^{0\nu}$ , and  $m_A^{0\nu}$  are usually written as  $m_F^{0\nu}$ , and  $m_{GT}^{0\nu}$ , and that the  $l=2$  parts in  $m_P^{0\nu}$ , and  $m_M^{0\nu}$  are the tensor components of  $M^{0\nu}$ .

The two-body radial integrals are defined as (see [22])

$$\mathcal{R}_{LL'}^X(p_1 n_1 p_2 n_2; \mathcal{D}) = r_N \int dk k^2 v_X(k; \mathcal{D}) \times R_L(p_1 n_1; k) R_{L'}(p_2 n_2; k), \quad (29)$$

with

$$R_L(pn; k) = \int_0^\infty u_{n_p l_p}(r) u_{n_n l_n}(r) j_L(kr) r^2 dr, \quad (30)$$

and

$$v_X(k; \mathcal{D}) = \frac{2}{\pi} \frac{\mathcal{G}_X(k)}{k(k+\mathcal{D})}, \quad (31)$$

where  $\mathcal{G}_X(k) = g_V^2(k), g_A^2(k), k^2 f_M^2(k),$  and  $k^2 g_P(k)[2g_A(k) - k^2 g'_P(k)]$ , for  $X = V, A, M,$  and  $P$ , respectively. The ratio  $r_N = 1.2A^{1/3}$  fm is introduced to make the  $0\nu\beta\beta$  NMEs dimensionless [70].

The  $\beta\beta$ -decay half-lives are evaluated from

$$[\tau(\mathcal{J}_f)]^{-1} = \mathcal{F}^2 |M(\mathcal{J}_f)|^2 G(\mathcal{J}_f), \quad (32)$$

where the  $\beta\beta$ -decay mode factors are  $\mathcal{F}_{2\nu} = 1$ , and  $\mathcal{F}_{0\nu} = \langle m_\nu \rangle$ , with  $\langle m_\nu \rangle$  given in natural units ( $\hbar = m_e = c = 1$ ).

The reaction matrix elements  $\langle \mathcal{J}_f | | \mathcal{D}_{\mathcal{J}\mathcal{J}}^\mp | | 0^+ \rangle$ , with  $J = 0, 1$ , and  $\mathcal{J} = 0, 2$ , are evaluated in the same way as the  $0\nu\beta\beta$  NME, and one obtains

$$M_{\mathcal{J}}^\mp(\mathcal{J}_f) \equiv \langle \mathcal{J}_f | | \mathcal{D}_{\mathcal{J}\mathcal{J}}^\mp | | 0^+ \rangle = \hat{J}^{-1} \sum_{p_1 n_1 p_2 n_2} \times \bar{\varrho}^\mp(p_1 n_1 p_2 n_2; J \mathcal{J}_f^+) W_{0JJ}(p_1 n_1) W_{0JJ}(p_2 n_2). \quad (33)$$

The total DCE transition strengths  $S_{\mathcal{J}\mathcal{J}}^{\{\mp 2\}}$  and  $S^{0\nu^\mp}$  are evaluated from (2) and (33), and from (8) and (10), respectively.

Finally, the  $Q$ -values for the  $\beta\beta^-$ -decay, and for the  $ee$ -capture, defined as

$$Q_{\beta\beta^-} = \mathcal{M}(Z, A) - \mathcal{M}(Z+2, A), \quad Q_{ee} = \mathcal{M}(Z, A) - \mathcal{M}(Z-2, A), \quad (34)$$

where the  $\mathcal{M}$ 's are the atomic masses, are obtained from

$$Q_{\beta\beta^-} = E_{0^+}^{\{0\}} - E_{0_1^+}^{\{-2\}} \quad Q_{ee} = E_{0^+}^{\{0\}} - E_{0_1^+}^{\{+2\}}. \quad (35)$$

The above observables are evaluated within different nuclear structure models. Among them, the  $pn$ -QRPA is currently the most widely used nuclear model for estimating the NMEs for the  $\beta\beta$ -decays to the ground state  $0_1^+$ <sup>3</sup>. We have recently developed a new nuclear model for the DCE processes, based on the Quasiparticle Tamm-Dancoff Approximation (QTDA) for the  $pn$  and  $2p2n$  excitations [40]. It is a natural extension of the original

<sup>3</sup> The SCE QRPA model was developed by Halbleib and Sorensen in 1967 [28] to describe the  $\beta$ -decay. Later, in the 1990s, averaging over two  $\beta$ -decays, this QRPA was adapted for  $\beta\beta$ -decay calculations [29–38]. The unfavorable aspects of the  $pn$ -QRPA model are that: 1) It cannot describe  $\beta\beta$ -decays to excited states, and 2) It does not allow the evaluation of the total strengths (2), and therefore neither the sum rules (5) nor the ratios  $R_{\mathcal{J}}^{\{\mp 2\}}(\mathcal{J}_f^+)$  given by (7), cannot be discussed either

QRPA [28], and will be labeled DCEQTDA<sup>4</sup>. The graphical representation of the two models is given in [40, Fig. 1]. The difference between them is cardinal, and has very important consequences, both analytical and numerical. Below, we present the corresponding formulation within the DCEQTDA.

## B. DCEQTDA Nuclear Model

The basic assumption in the DCEQTDA is that the nuclei  $(A, Z)$ ,  $(A, Z \pm 1)$  and  $(A, Z \pm 2)$  can be represented, respectively, as the BCS vacuum, and the excitations of two  $pn$  and four  $2p2n$  quasiparticles in this vacuum. The resulting eigenvalue problem is discussed in details in our previous work [40]. Here, we only deal we the resulting wave functions

$$\begin{aligned} |J_i\rangle &= \sum_{p_1 n_1} X_{p_1 n_1 J_i} |p_1 n_1 J\rangle, \\ |\mathcal{J}_f\rangle &= \sum_{p_1 p_2 n_1 n_2} \mathcal{X}_{p_1 p_2 J_p, n_1 n_2 J_n; \mathcal{J}_f} |p_1 p_2 J_p, n_1 n_2 J_n; \mathcal{J}\rangle, \end{aligned} \quad (36)$$

and the corresponding energies  $\omega_{J_i}$  and  $\Omega_{\mathcal{J}_f}$ , for the intermediate and final nuclei, respectively.

The two-body density matrix  $\varrho^-(p_1 n_1 p_2 n_2; J_i, \mathcal{J}_f)$  are evaluated from (14), with the result

$$\begin{aligned} \varrho^-(p_1 n_1 p_2 n_2; J_i \mathcal{J}_f^+) &= \hat{J} \hat{\mathcal{J}}_f \\ &\times \sum_{pn J_p J_n} (-)^{J_p + J_n} \hat{J}_p \hat{J}_n N(nn_2) N(pp_2) \\ &\times \mathcal{X}_{pp_2 J_p, nn_2 J_n; \mathcal{J}_f} \bar{P}(nn_2 J_n) \bar{P}(pp_2 J_p) \\ &\times \begin{Bmatrix} p & p_2 & J_p \\ n & n_2 & J_n \\ J & J & \mathcal{J} \end{Bmatrix} u_{p_2} v_{n_2} X_{pn J_i} u_{p_1} v_{n_1} X_{p_1 n_1 J_i} \end{aligned} \quad (37)$$

where  $\hat{J} = \sqrt{2J+1}$ , and

$$N(ab) = (1 + \delta_{ab})^{-1/2}, \quad (38)$$

is the two particles normalization factor. The operator

$$\bar{P}(p_1 p_2 J) = 1 + (-)^{p_1 - p_2 + J} P(p_1 \leftrightarrow p_2), \quad (39)$$

takes into account the Pauli Principle by exchanging the particles  $p_1$  and  $p_2$ , and acts only on the right hand side.

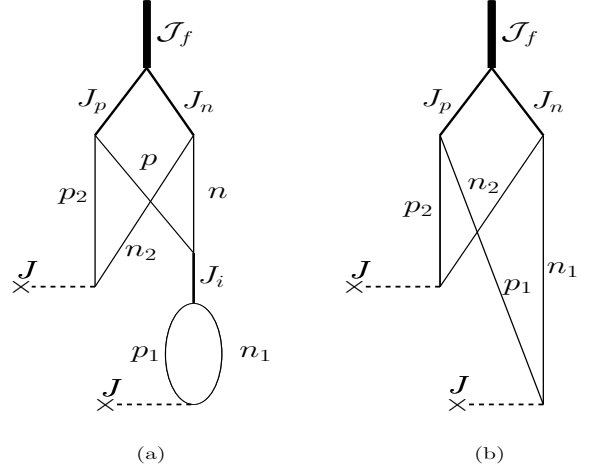


FIG. 1: Two-body transition densities  $\varrho(p_1 n_1 p_2 n_2; J_i \mathcal{J}_f)$ , given by (37) and used in the evaluation of  $M^{2\nu}(\mathcal{J}_f)$ , and  $\bar{\varrho}(p_1 n_1 p_2 n_2; J J_f)$ , given by (40), and used to calculate  $M^{0\nu}(0_f^+)$  within the CA and to  $M_J(\mathcal{J}_f)$ , are shown in panels (a) and (b), respectively. The dashed lines indicate the single  $\beta$ -decays. The first  $\beta$ -decay is activated in the initial state, and the second in the intermediate state. The five vertices of these diagrams correspond to five of the six angular momentum couplings in the symbol  $9j$  in Eqs. (37) and (40). The sixth coupling  $(JJ)\mathcal{J}$  corresponds to the three unconnected lines.

Moreover, from (37)

$$\begin{aligned} \bar{\varrho}^-(p_1 n_1 p_2 n_2; J \mathcal{J}_f) &= \hat{J} \hat{\mathcal{J}}_f \\ &\times \sum_{J_p J_n} (-)^{J_p + J_n} \hat{J}_p \hat{J}_n N(n_1 n_2) N(p_1 p_2) \\ &\times \mathcal{X}_{p_1 p_2 J_p, n_1 n_2 J_n; \mathcal{J}_f} \bar{P}(n_1 n_2 J_n) \bar{P}(p_1 p_2 J_p) \\ &\times \begin{Bmatrix} p_1 & p_2 & J_p \\ n_1 & n_2 & J_n \\ J & J & \mathcal{J} \end{Bmatrix} u_{p_2} v_{n_2} u_{p_1} v_{n_1}. \end{aligned} \quad (40)$$

The corresponding density matrices  $\varrho^+(p_1 n_1 p_2 n_2; J_i, \mathcal{J}_f)$ , and  $\bar{\varrho}^+(p_1 n_1 p_2 n_2; J_i \mathcal{J}_f)$  are obtained from (37), and (40), respectively, after making  $u_{p_1} v_{n_1} \rightarrow u_{n_1} v_{p_1}$ , and  $u_{p_2} v_{n_2} \rightarrow u_{n_2} v_{p_2}$ .

The graphical representations of densities  $\varrho(p_1 n_1 p_2 n_2; J_i^\pi \mathcal{J}_f^+)$ , and  $\bar{\varrho}(p_1 n_1 p_2 n_2; J_i^\pi \mathcal{J}_f^+)$  are exhibited, respectively, in panels (a), and (b) of Fig. 1.

The energies of the intermediate state  $|J_i\rangle$  and the final state  $|\mathcal{J}_f\rangle$ , relative to the initial state  $|0^+\rangle$ , are

$$\begin{aligned} E_{J_i}^{\{\mp 1\}} - E_{0^+}^{\{0\}} &= \omega_{J_i} \pm \lambda_p \mp \lambda_n, \\ E_{\mathcal{J}_f}^{\{\mp 2\}} - E_{0^+}^{\{0\}} &= \Omega_{\mathcal{J}_f} \pm 2\lambda_p \mp 2\lambda_n, \end{aligned} \quad (41)$$

where  $\lambda_p$  and  $\lambda_n$  are the proton and neutron chemical potentials. Therefore, the energy denominator (16) becomes

$$\mathcal{D}_{J_i, \mathcal{J}_f} = \omega_{J_i} - \frac{\Omega_{\mathcal{J}_f}}{2}, \quad (42)$$

<sup>4</sup> This model has been proposed, and applied in its particle-hole limit for  $\beta\beta$ -decay in <sup>48</sup>Ca, long years ago [39].

being the same for  $\beta\beta^\mp$ -decays.

The  $Q$ -values, for the  $\beta\beta^-$ -decay and for the  $ee$ -capture, in present model, are given by

$$\begin{aligned} Q_{\beta\beta^-} &= -\Omega_{0_1^+} - 2(\lambda_p - \lambda_n), \\ Q_{ee} &= -\Omega_{0_1^+} + 2(\lambda_p - \lambda_n). \end{aligned} \quad (43)$$

These are the windows of excitation energies where  $\beta\beta$ -decay can be observed. Note that their difference

$$\Delta Q \equiv Q_{ee} - Q_{\beta\beta^-} = 4(\lambda_p - \lambda_n), \quad (44)$$

depends only on the mean field.

### III. NUMERICAL RESULTS AND DISCUSSION

#### A. Residual Interaction and Single Particle Energies

We describe the residual interaction with the  $\delta$ -force

$$V = -4\pi(v^s P_s + v^t P_t)\delta(r) \quad \text{MeV}\cdot\text{fm}^3, \quad (45)$$

for its simplicity, and because in this way the comparison can be made between the present DCEQTDA and our previous  $pn$ -QRPA calculations of the NMEs, shown in Fig. 3 of Ref. [26].

To highlight the differences between the two models, we will use here the same parameterization that was used in the  $pn$ -QRPA:

1) The pairing strengths for protons and neutrons,  $v_{\text{pair}}^s(p)$  and  $v_{\text{pair}}^s(n)$  were obtained from the fitting of the corresponding experimental pairing gaps.

2) The isovector ( $v^s$ ) and isoscalar ( $v^t$ ) parameters within the particle-particle (pp) and particle-hole (ph) channels, as well as the ratios  $s = v_{\text{pp}}^s/\bar{v}_{\text{pair}}^s$ , and  $t = v_{\text{pp}}^t/\bar{v}_{\text{pair}}^s$ , with  $\bar{v}_{\text{pair}}^s = (v_{\text{pair}}^s(p) + v_{\text{pair}}^s(n))/2$ , were fixed in the same way as in our QRPA calculations [26, 40] (see [26, Fig. 1]. That is, they are determined from the condition that the strengths  $S_f^{\{+1\}}$  become minimal, with the result  $s = s_{\text{sym}} = 1$ , and  $t = t_{\text{sym}} \gtrsim 1$ , and which is named Partial SU(4) Symmetry Restoration (PSU4SR).

In the present case we have  $t_{\text{sym}} = 1.34$  for  $^{76}\text{Ge}$ , and  $t_{\text{sym}} = 1.42$  for  $^{124}\text{Xe}$ . This parametrization will be labeled as P1. We have found it convenient to show in the case of  $^{76}\text{Ge}$  also the results for the value of the parameter  $t$  that reproduces the measured value of the ground state  $2\nu$  NME. This is frequently done in the literature [25], with the result here  $t = 1.86$ , which we will label as P2.

All NMEs were evaluated with the measured value  $g_A = 1.27$  [44]. The  $\beta\beta$ -decay half-lives were calculated from (28), and all kinematics factors  $G_{2\nu}(\mathcal{J}_f^+)$ , and  $G_{0\nu}(\mathcal{J}_f^+)$  were taken from [46], except for  $G_{2\nu}(2_2^+)$  in  $^{76}\text{Ge}$  that was found in [47].

In order to satisfy the sum rules (4) and (5) it is necessary to work with a sufficiently large number of single-particle states, which have to be the same for protons

and neutrons, and spin-orbit partners must always be included. The corresponding single-particle energies were obtained from the Wood-Saxon potential with the standard [48] parameterization.

Thus, we use 9 single-particle levels ( $2d_{3/2}$ ,  $1g_{7/2}$ ,  $3s_{1/2}$ ,  $2d_{5/2}$ ,  $1g_{9/2}$ ,  $2p_{1/2}$ ,  $1f_{5/2}$ ,  $2p_{3/2}$ , and  $1f_{7/2}$ ) in  $^{76}\text{Ge}$ , and 7 levels ( $1h_{9/2}$ ,  $1h_{7/2}$ ,  $2d_{3/2}$ ,  $1g_{7/2}$ ,  $3s_{1/2}$ ,  $2d_{5/2}$ , and  $1g_{9/2}$ ) in  $^{124}\text{Xe}$ . The number of resulting four quasiparticle states  $|\mathcal{J}^+\rangle$ , defined in (36), are 2045 states  $|0^+\rangle$ , and 8456 states  $|2^+\rangle$  in  $^{76}\text{Ge}$ , and 1146 states  $|0^+\rangle$ , and 4918 states  $|2^+\rangle$  in  $^{124}\text{Te}$ . Some calculations have been performed on this nucleus with 9 levels, including also the states  $1f_{7/2}$  and  $1f_{5/2}$ .

#### B. Measured DCE Observables

TABLE I: Calculated and experimental  $Q$ -values (in MeV) for  $^{76}\text{Ge}$ . The parameterizations P1, and P2 are explained in the text.

Par/Exp	$Q_{\beta\beta^-}$	$Q_{ee}$	$\Delta Q$
$^{76}\text{Ge}$			
P1	1.239	-8.240	-9.479
P2	1.314	-8.164	-9.478
Exp. [49]	2.039	-10.910	-12.95
$^{124}\text{Xe}$			
P1	-9.403	4.071	13.474
Exp. [49]	-8.572	2.864	11.436

First, we will focus on the DCE observables that have been experimentally measured, and will serve to test the nuclear model used. This will be done for the  $\beta\beta$ -decay in  $^{76}\text{Ge}$ , and for the  $ee$ -capture in  $^{124}\text{Xe}$ , analyzing:

a) The  $Q$ -values, defined in (34), that are given in Table I, The agreement between the data and the calculations is quite reasonable. It should be noted that we obtain that  $Q_{\beta\beta^-}$  is positive and  $Q_{ee}$  negative for  $^{76}\text{Ge}$ , and opposite for  $^{124}\text{Xe}$ , which, although expected, is not a trivial result.

b) The excitation energies  $\mathcal{E}_{\mathcal{J}_f^+}$  in the final nuclei, and the  $2\nu$  NMEs for  $\mathcal{J}_f^+ = 0_{1,2}^+$ , and  $2_{1,2}^+$ , both are listed in Table II. All energies are reasonably well reproduced, except  $\mathcal{E}_{2_1^+}$  in  $^{124}\text{Te}$ , which turned out to be negative. This fact may be due to the fact that we are not considering the collective (vibrational) degrees of freedom, which play an important role in even Te isotopes. <sup>5</sup>

<sup>5</sup> This has been known for a long time. In fact, in Ref. [52] the nuclear structure of the even isotopes of Te is discussed in the framework of the semimicroscopic particle-phonon model.

TABLE II: Calculated and experimental excitation energies  $\mathcal{E}_{\mathcal{J}_f}$  in  $^{76}\text{Ge}$ , the NMEs  $M^{2\nu}(\mathcal{J}_f^+)$ , and half-lives  $\tau_{2\nu}(\mathcal{J}_f^+)$  for the decays of  $^{76}\text{Ge}$ , and  $^{124}\text{Xe}$  to  $\mathcal{J}_f^+ = 0_{1,2}^+$ , and  $2_{1,2}^+$  states in  $^{76}\text{Se}$ , and  $^{124}\text{Te}$ , respectively, with parameterizations P1 and P2, and with  $g_A = 1.27$  [44]. This table also shows the calculations in  $^{76}\text{Ge}$  performed within: i) the Multiple-Commutator Model (MCM), [68], and ii) the Shell Model (SM) [67], as well as the calculations in  $^{124}\text{Xe}$  performed within: i) MCM [50], and ii) the Effective Theory (ET), and the SM [51], where all NMEs are multiplied by  $(g_A = 1.27)^2$ . The experimental ground state  $\tau_{2\nu}^{ee}(\mathcal{J}_f^+)$  is from Ref. [17]. The measured half-lives in  $^{76}\text{Se}$  are from [53] for the ground state, and from [7] for the excited states, and the experimental  $\tau_{2\nu}^{ee}$  in  $^{124}\text{Te}$  is from Ref. [17]. All  $G$  factors are from Ref. [46], except that of the  $2_2^+$  state in  $^{76}\text{Se}$ , which is from Ref. [47].

$^{76}\text{Ge} \rightarrow ^{76}\text{Se}$	$\mathcal{J}_f^+$	$0_1^+$	$0_2^+$	$2_1^+$	$2_2^+$
$\mathcal{E}$ (MeV)					
	P1	0.0	2.13	0.36	1.98
	P2	0.0	2.13	0.26	1.90
	Exp.	0.0	1.12	0.56	1.22
$ M^{2\nu} $ (n.u.)		$\times 10^3$	$\times 10^3$	$\times 10^3$	$\times 10^3$
	P1	56.4	80.1	2.8	5.2
	P2	103	158	6.6	12.3
	SM	97	70	0.7	1.8
	MCM	74	363	1	3
	Exp.	107	< 147	< 58	< 873
$\tau_{2\nu}$ (yr)		$\times 10^{21}$	$\times 10^{23}$	$\times 10^{23}$	$\times 10^{24}$
	P1	6.8	25	$3.3 \cdot 10^3$	$3.6 \cdot 10^4$
	P2	2.0	6.5	$6.0 \cdot 10^2$	$6.5 \cdot 10^3$
	Exp.	1.88	> 7.5	> 7.7	> 1.3
$^{124}\text{Xe} \rightarrow ^{124}\text{Te}$	$\mathcal{J}_f^+$	$0_1^+$	$0_2^+$	$2_1^+$	$2_2^+$
$\mathcal{E}$ (MeV)					
	P1	0.0	1.74	-0.16	1.62
	Exp.	0.0	1.66	0.60	1.32
$ M^{2\nu} $ (n.u.)		$\times 10^3$	$\times 10^3$	$\times 10^3$	$\times 10^3$
	P1	62	46	7.1	8.3
	ET	18 – 66	3.2 – 80	0.13 – 1.45	
	SM	45 – 116	8 – 16	0.17 – 0.37	
	MCM	476	15	1.1	0.11
	Exp.	$57 \pm 10$			
$\tau_{2\nu}$ (yr)		$\times 10^{22}$	$\times 10^{25}$	$\times 10^{28}$	
	P1	1.51	0.28	0.14	
	ET	18.6 – 1.33	57.8 – 0.92	435 – 3.45	
	SM	2.87 – 0.43	9.21 – 2.34	231 – 52.6	
	MCM	0.026	2.66	5.99	
	Exp.	$1.8 \pm 0.5$			

c) The ground state NMEs,  $M^{2\nu}(0_1^+)$ , are also well reproduced in both nuclei.

d) The corresponding half-lives  $\tau_{2\nu}$  are also shown, and compared with the experimental data [6, 17, 53]. All our computed half-lives  $\tau_{2\nu}(\mathcal{J}_f^+)$  are consistent with the measurements.

For comparison, Table II further shows the calculations in  $^{76}\text{Ge}$  performed within: i) the Multiple-Commutator Model (MCM), the Shell Model (SM) [67], as well as the calculations in  $^{124}\text{Xe}$  performed within: i) MCM [50], and ii) the Effective Theory (ET), and the SM [51].

### C. $0\nu\beta\beta$ NMEs

#### 1. Anatomy of $0\nu\beta\beta$ NMEs

In Table III we show the contributions of different intermediate states  $J^\pi$  to  $M^{0\nu^-}(0_1^+)$  in  $^{76}\text{Se}$  (positive parities in the top panel and negative parities in the bottom panel, evaluated in the  $pn$ -QRPA and DCEQTDA, with the same residual interaction (45) and the parametrization P1, and using the same set of single-particle energies in both cases. The most relevant numbers are shown in

TABLE III: Fine structure of  $M^{0\nu}(0_1^+)$  for  $^{76}\text{Ge}$ , evaluated in the  $pn$ -QRPA and DCEQTDA with the same parametrization P1 in both cases. The contributions of different intermediate-state angular momenta  $J^\pi$  are listed for both parities  $\pi = \pm$ . The most relevant numbers are shown in bold type.

$J^\pi$	$pn$ -QRPA					DCEQTDA				
	$M_V^{0\nu}$	$M_A^{0\nu}$	$M_M^{0\nu}$	$M_P^{0\nu}$	$M^{0\nu}$	$M_V^{0\nu}$	$M_A^{0\nu}$	$M_M^{0\nu}$	$M_P^{0\nu}$	$M^{0\nu}$
$0^+$	<b>0.020</b>	0.000	0.000	0.000	0.020	<b>0.145</b>	0.000	0.000	0.000	0.145
$1^+$	0.000	<b>-0.682</b>	0.007	-0.022	-0.697	0.000	<b>0.466</b>	0.006	-0.027	0.445
$2^+$	0.173	0.255	0.026	0.000	0.453	0.035	0.047	0.005	0.000	0.087
$3^+$	0.000	0.475	0.028	-0.172	0.330	0.000	0.077	0.004	-0.018	0.064
$4^+$	0.080	0.121	0.022	0.000	0.223	0.011	0.014	0.003	0.000	0.027
$5^+$	0.000	0.230	0.024	-0.104	0.150	0.000	0.026	0.003	-0.008	0.021
$6^+$	0.030	0.049	0.015	0.000	0.093	0.003	0.004	0.001	-0.000	0.008
$7^+$	0.000	0.097	0.014	-0.045	0.066	0.000	0.009	0.001	-0.003	0.007
$8^+$	0.009	0.014	0.005	0.000	0.028	0.001	0.001	0.000	0.000	0.002
$9^+$	0.000	0.056	0.012	-0.026	0.042	0.000	0.006	0.001	-0.002	0.005
$\pi = +$	0.311	0.613	0.153	-0.368	0.708	0.194	0.650	0.024	-0.057	0.811
$0^-$	0.000	0.054	0.000	-0.029	0.025	0.000	0.009	0.000	-0.003	0.006
$1^-$	0.149	0.227	0.013	0.000	0.389	0.019	0.023	0.001	0.000	0.043
$2^-$	0.000	0.741	0.025	-0.170	0.596	0.000	0.148	0.004	-0.017	0.135
$3^-$	0.107	0.230	0.031	0.000	0.368	0.011	0.028	0.004	0.000	0.043
$4^-$	0.000	0.398	0.033	-0.144	0.286	0.000	0.048	0.004	-0.009	0.043
$5^-$	0.060	0.132	0.031	0.000	0.223	0.006	0.015	0.003	-0.000	0.024
$6^-$	0.000	0.201	0.027	-0.084	0.144	0.000	0.018	0.002	-0.004	0.016
$7^-$	0.028	0.064	0.023	0.000	0.115	0.003	0.006	0.002	0.000	0.012
$8^-$	0.000	0.050	0.010	-0.023	0.037	0.000	0.002	0.000	-0.000	0.002
$\pi = -$	0.343	2.098	0.193	-0.451	2.183	0.039	0.296	0.021	-0.034	0.323
Total	<b>0.654</b>	<b>2.711</b>	0.346	-0.819	<b>2.891</b>	<b>0.234</b>	<b>0.946</b>	0.045	-0.091	<b>1.133</b>

bold type. <sup>6</sup>

It is important to note that the  $0\nu\beta\beta$  NMEs differ from the  $2\nu\beta\beta$  and reaction NMEs not only in radial dependence, but also in genesis. Indeed, while they receive contributions from all intermediate states  $J^\pi = 0^\pm, 1^\pm, \dots, 9^\pm$ , the latter are constructed only from the intermediate states  $J^\pi = 0^+(M_V^{2\nu}, \text{ and } M_{00})$ , and  $J^\pi = 1^+(M_A^{2\nu}, \text{ and } M_{10})$ .

The most remarkable difference between the two calculations is that: i) while in the  $pn$ -QRPA calculation the contributions of the intermediate states with  $J^\pi \neq 1^+$  are much bigger than those of the  $J^\pi = 1^+$  states, and that they are of opposite sign, ii) in the DCEQTDA calculation the contributions of the intermediate states with  $J^\pi \neq 1^+$  are smaller than those of the  $J^\pi = 1^+$  states, and that all spins contribute coherently. The final result is that the total  $0\nu\beta\beta$  NME  $M^{0\nu}$  is factor of 3 lower than the one obtained in the  $pn$ -QRPA calculation.

Comparing with similar calculations performed previ-

ously we see that:

a) Our results with  $pn$ -QRPA agree both qualitatively and quantitatively with calculations performed by Šimković, *et al.*[73, Fig. 3], employing the same nuclear model, while

b) The calculations performed in the DCEQTDA are consistent with the SM results obtained by Sen'kov and Horoi [74, Fig. 3].

To facilitate the comparison of the results of Refs. [73, 74] with ours, in Fig. 2 we show the total contributions of each intermediate state  $J^\pi$  to  $M^{0\nu}(0_1^+)$  in  $^{76}\text{Se}$  (positive parities in the upper panel and negative in the lower panel, evaluated in the same way as in Table III.

From the results shown above, one can infer that in a nuclear structure calculation the central role is played by the degrees of freedom included in the model, while the details of the nuclear force employed are of minor importance. In this case, the Pauli Principle in the final nucleus is that produces the big difference between the DCEQTDA and  $pn$ -QRPA results.

<sup>6</sup> With the P2 parameterization, similar results are obtained in the DCEQTDA, but the  $pn$ -QRPA in this case collapses.



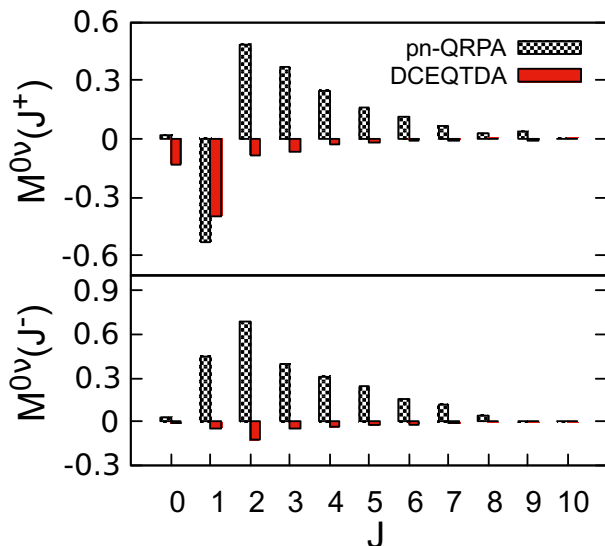


FIG. 2: Contributions of different intermediate-state angular momenta  $J^\pi$  to  $M^{0\nu}(0_1^+)$  in  $^{76}\text{Se}$  within  $pn$ -QRPA and DCEQTDA nuclear models employing the same parametrization P2. Positive parities are shown in the upper panel and negative parities in the lower one.

## 2. Comparison with other calculations of $0\nu\beta\beta$ NMEs

The upper part of Table IV presents the comparison between the calculated  $0\nu\beta\beta$  NMEs for the  $\mathcal{J}_f^+ = 0_{1,2}^+$  states in  $^{76}\text{Se}$  with the P1 and P2 parameterizations. When compared with the calculation of the  $2\nu\beta\beta$ -decay from Table II, it is observed that the differences between the two results here are relatively smaller. On the other hand, as expected both current values of  $M^{0\nu}(0_1^+)$  in  $^{76}\text{Ge}$  are notably smaller than those obtained in our  $pn$ -QRPA calculation [26], which was  $M^{0\nu}(0_1^+) = 3.19_{-0.24}^{+0.46}$ .

The present  $0\nu\beta\beta^-$  NMEs are also much smaller than those obtained in several previous calculations, as shown, for example, in [26, Fig. 3]. In particular, the  $pn$ -QRPA calculations done with more realistic forces, such as Argonne V18 or CD-Bonn potentials [55, 56], lead to  $M^{0\nu}(0_1^+) \cong 5.5$ . It should also be noted that there is a recent work with *ab-initio* calculations from chiral EFT [57] that goes in the same direction as our calculations, obtaining  $M^{0\nu}(0_1^+) = 2.14$ .

Using the calculated NMEs in  $^{76}\text{Ge}$ , together with the measured half-lives:  $\tau_{0\nu}(0_1^+) > 1.8 \cdot 10^{26}$  yr [6], and  $\tau_{0\nu}(0_2^+) > 7.5 \cdot 10^{23}$  yr [7], and the  $G(0_{1,2}^+)$  factors from [46], we get from (32) the lower limits for  $\langle m_\nu \rangle$ , that are shown in the last column of Table IV.

In the lower part of Table IV are presented the  $0\nu ee$ -capture NMEs for the  $\mathcal{J}_f^+ = 0_{1,2}^+$  final states in  $^{124}\text{Te}$ , evaluated with 7 and 9 single-particle levels, obtainin

quite similar results. In both cases, they are noticeably smaller than our  $0\nu\beta\beta^-$ -decay NMEs for  $^{76}\text{Se}$ .

We have also performed the calculations on  $^{78}\text{Kr}$  and  $^{130}\text{Ba}$  nuclei, where the  $0\nu ee$ -capture occurs, reaching the same conclusion. That is, the present model says that the NMEs are about an order of magnitude smaller in the  $0\nu ee$ -capture than in the  $0\nu\beta\beta^-$ -decay. This is fully consistent with Eq. (15), but strongly disagrees with the  $pn$ -QRPA and IBM calculations shown in [58, Table IV]. It should be noted that the relations (15) are completely independent of the nuclear model used, and depend only on the neutron excess.

A more complete calculation of the  $0\nu\beta\beta^-$  and  $0\nu ee$  NMEs will be presented in a future article.

## 3. Relation between $0\nu\beta\beta$ , and DF and DGT NMEs

At the top of Table IV, we confront:

- i) The  $0\nu\beta\beta$  NMEs  $M_V^{0\nu}$ ,  $M_{V_{0^+}}^{0\nu}$ ,  $M_A^{0\nu}$ ,  $M_{A_{1^+}}^{0\nu}$ ,  $M_P^{0\nu}$ ,  $M_M^{0\nu}$ , and  $M^{0\nu}$ , with
- ii) The absolute values of  $M_{00}$ , and  $M_{10}$ .

From the discussion presented above in Section III C 1, it is easy to be convinced that physically  $M_{00}$  corresponds to  $M_{V_{0^+}}^{0\nu}$ , since both are generated only from intermediate states  $J = 0^+$ . The same is true for  $M_{10}$  and  $M_{A_{1^+}}^{0\nu}$ , which are generated only from intermediate states  $J = 1^+$ . Therefore it is not correct to associate  $M_{00}$  with  $M_V^{0\nu}$ , nor  $M_{10}$  with  $M_A^{0\nu}$ , as is often done.

The fact that  $0\nu\beta\beta$  and DCER NMEs turn out to be of the same order of magnitude is a surprise in view of the large differences between them (radial and energy dependencies, finite nucleon size effects, and short-range correlations taken into account in the former, etc). It should also be remembered that the nuclear radius  $r_N$  was introduced into  $M^{0\nu}$  by Doi [70] some time ago in a rather arbitrary way, just to make it dimensionless (see (29)).

In previous comparisons between  $M_{10}$  and  $M^{0\nu}$  [13–16], the results obtained for them in different calculations and with different nuclear models were used. In addition, the contributions of the NMEs: V, P and M to  $M^0$ , which, although small, are significant, were omitted.

## D. DCE Sum Rules, and Calibration of NMEs

To verify the sum rules (5) we have to evaluate from (2) the total reaction strengths  $S_{J\mathcal{J}}^{\{\mp 2\}}$ , and then their differences  $S_{J\mathcal{J}}^{\{2\}}$  from (2). This will allow us to calibrate the NMEs  $M_{J\mathcal{J}}$  from (7). But, to calibrate the the NMEs  $M_V^{0\nu}$ , and  $M_A^{0\nu}$  from (11), we also need to know the total and vector and axial vector strengths  $S_{V,A}^{0\nu\mp}$ .

All results for the DCE transition strengths in  $^{76}\text{Ge}$ , and  $^{124}\text{Xe}$  are summarized in Table V. We also show

TABLE IV: At the top is the comparison between the NMEs  $M^{0\nu^-}(0_f^+) \equiv M^{0\nu}$ , and  $M_{J\mathcal{J}}^-(0_f^+) \equiv M_{J\mathcal{J}}$ , for the  $0_f^+ = 0_{1,2}^+$  states in  $^{76}\text{Se}$ , within the parameterizations P1 and P2. The upper bounds of  $\langle m_\nu \rangle$  are evaluated from Eq. (32), and are given in units of eV. In doing so, we have used the measured half-lives:  $\tau_{0\nu}(0_1^+) > 1.8 \times 10^{26}$  yr [6], and  $\tau_{0\nu}(0_2^+) > 4 \times 10^{23}$  yr [7]. The lower part of the table shows the same but only the NMEs  $M^{0\nu^+}(0_f^+) \equiv M^{0\nu}$  for electron capture in the  $0_f^+ = 0_{1,2}^+$  states of  $^{124}\text{Te}$ , obtained with 7, and 9 single-particle levels. In this case we do not make the comparison with reaction NMEs. All NMEs are multiplied by  $10^3$ .

$0_f^+$	$M_V^{0\nu}$	$M_{V_{0^+}}^{0\nu}$	$ M_{00} $	$M_A^{0\nu}$	$M_{A_{1^+}}^{0\nu}$	$ M_{10} $	$M_P^{0\nu}$	$M_M^{0\nu}$	$M^{0\nu}$	$\langle m_\nu \rangle$
$^{76}\text{Se}$										
P1										
$0_1^+$	234	145	221	946	466	399	-91	45	1133	0.69
$0_2^+$	168	106	170	826	457	419	-72	33	955	60.9
P2										
$0_1^+$	-296	-198	305	-1176	-650	573	105	-50	-1417	0.55
$0_2^+$	211	144	234	1030	635	594	-82	36	1195	48.6
$^{124}\text{Te}$										
7 levels										
$0_1^+$	34		133			-14	8.0	162		
$0_2^+$	5.7		6.8			-3.4	1.0	10		
9 levels										
$0_1^+$	42.9		142			-15	8.4	178		
$0_2^+$	-9.3		-5.2			-3.0	-0.9	-12		

results for the partial vector and axial-vector strengths  $S_{V_{0^+,A_{1^+}}}^{0\nu^\mp}$ , both defined in (10).

We have found that:

- 1) In the case of  $^{76}\text{Ge}$ , identical results are obtained with parameterizations P1 and P2.
- 2) In the case of  $^{124}\text{Xe}$ , both calculations with 7 and 9 single-particle states satisfy the sum rules (5).
- 3) To satisfy the conditions in Eq. (6), it is essential to include the term  $2S_1^{\{-1\}}$  in (5); otherwise, for example, in  $^{76}\text{Ge}$ , instead of  $S_{10}^{\{2\}} = 353$ , we obtain  $S_{10}^{\{2\}} = 312$ .
- 4) Since  $S_{J\mathcal{J}}^{\{2\}}$  is independent of the nuclear model, the result  $S_{J\mathcal{J}}^{\{2\}} \cong S_{J\mathcal{J}}^{\{2\}}$  implies that the DCER sum rules are well satisfied, which in turn means that the reaction transition strengths  $S_{J\mathcal{J}}^{\{-2\}}$ , and  $S_{J\mathcal{J}}^{\{+2\}}$  are evaluated correctly. Then, it is reasonable to assume that the results for the total transition strengths  $S_{V,A}^{0\nu^\mp}$ , and  $S_{V_{0^+,A_{1^+}}}^{0\nu^\mp}$  are also correct.
- 5) Since the term proportional to  $C$  is not taken into account when evaluating  $S_{10}^{\{2\}}$ , and  $S_{12}^{\{2\}}$  using (5), the inequalities (6) are satisfied as expected.
- 6) While  $S_{V_{0^+,A_{1^+}}}^{0\nu^-}$  are only slightly smaller than  $S_{V,A}^{0\nu^-}$ ,  $S_{V_{0^+,A_{1^+}}}^{0\nu^+}$  are very small compared to  $S_{V,A}^{0\nu^+}$ . In both cases

TABLE V: Results for the DCER strengths  $S_{J\mathcal{J}}^{\{\mp 2\}}$ , and the  $0\nu\beta\beta^\mp$ -decay strengths  $S_{V,A}^{0\nu^\mp}$ , and  $S_{V_{0^+,A_{1^+}}}^{0\nu^\mp}$ , in  $^{76}\text{Ge}$ , and  $^{124}\text{Xe}$ . In the case of  $^{76}\text{Ge}$  identical results are obtained with parameterizations P1 and P2. The inequalities in this table are due to the fact that the  $C$  terms in (5) are not included in the calculations.

$J\mathcal{J}$	$S_{J\mathcal{J}}^{\{-2\}}$	$S_{J\mathcal{J}}^{\{+2\}}$	$S_{J\mathcal{J}}^{\{2\}}$	$S_{J\mathcal{J}}^{\{2\}}$	$S_{V,A}^{0\nu^-}$	$S_{V_{0^+,A_{1^+}}}^{0\nu^-}$	$S_{V,A}^{0\nu^+}$	$S_{V_{0^+,A_{1^+}}}^{0\nu^+}$
$^{76}\text{Ge}$								
00	300	0.56	299	264	135	128	1.9	0.23
10	330	1.4	328	$\leq 353$	469	375	36	1.6
12	1536	6.7	1529	$\geq 1403$				
$^{124}\text{Xe}$								
7 levels								
00	549	1.5	548	480	221	217	2.3	0.55
10	641	6.7	634	$\leq 661$	753	673	43	7.0
12	2996	31.0	2965	$\geq 2827$				
9 levels								
00	558	2.0	556	480	231	220	3.3	0.71
10	653	8.0	645	$\leq 672$	826	685	57	8.1

the partial strengths  $S_{V_{0^+,A_{1^+}}}^{0\nu^\mp}$  are similar in magnitude to their reaction counterparts  $S_{J_0}^{\{\mp 2\}}$ . In particular,

$$S_{10}^{\{\mp 2\}} \cong S_{A_{1^+}}^{0\nu^\mp},$$

which is consistent with  $|M_{10}| \cong |M_{A_{1^+}}^{0\nu}|$  reported earlier in Table IV. That is, the total transition intensities of the DGT NMEs are congruent to those of the  $0\nu$  axial-vector NMEs that are engendered from the  $1^+$  intermediate states (see also the Fig. 2).

7) From the above results we can now calibrate the NMEs, evaluating the amounts of the total strengths that are concentrated in the ground state, which are defined in Eqs. (7), and (11).

They are shown in Table VI for  $^{76}\text{Ge}$ . All ratios  $R$  are of the order of  $10^{-4} - 10^{-3}$ . These results are fully consistent with the findings of Auerbach *et al.*[3–5], who concluded, from the shell-model study of the  $2\nu\beta\beta^-$ -decay in  $^{48}\text{Ca}$ , that for the DGT is  $R_{10}^-(0_1^+) \sim (10^{-4} - 10^{-3})$ .

The above ratios are even smaller in  $0\nu ee$ -capture processes. For instance, for the ground state in  $^{124}\text{Te}$  with 7 levels we get  $R^{0\nu} = 6.9 \cdot 10^{-4}$ .

TABLE VI: Values of the ratios of the strengths defined in (7), and (11) for the ground state in  $^{76}\text{Se}$ , using the parameterizations P1 and P2. All the ratios are multiplied by  $10^3$ .

	$R_{00}^-$	$R_{10}^-$	$R_V^{0\nu}$	$R_A^{0\nu}$	$R^{0\nu}$
P1	0.29	0.99	6.4	2.9	2.1
P2	0.18	0.66	4.1	1.9	3.3

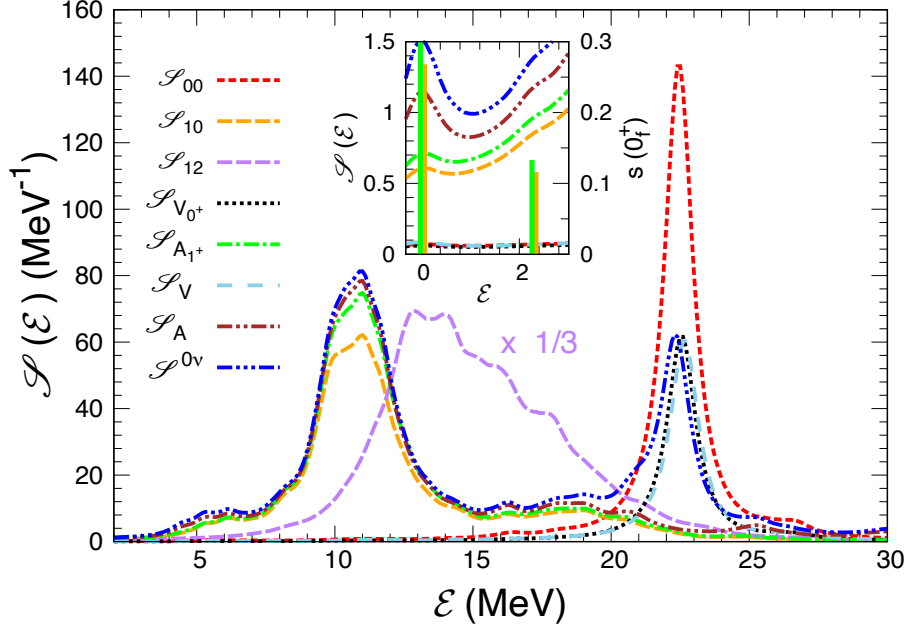


FIG. 3: The folded strength distributions  $\mathcal{S}^{\{-2\}}$  for the DCER and the  $0\nu\beta\beta$ -decay are shown as a function of the excitation energy  $\mathcal{E}$  in the final nucleus  ${}^{76}\text{Se}$ . The intensities  $s_{10}^{\{-2\}}$ ,  $s_{A_{1+}}^{0\nu^-}$ , and  $s^{0\nu^-}$  of the  $0_{1,2}^+$  states are shown in the inset plot.

### E. DCE Giant Resonances

The comparison made in Table IV between NMEs is now extended to the full strength distributions of the  $0\nu\beta\beta$ -decay and DCER NMEs, plotting their squares as a function of the excitation energies  $\mathcal{E}_f$ . Thus, we show in Figure 3 the folded transition densities  $\mathcal{S}$ , defined in (12), for the strengths  $s_{00}, s_{10}, s_{12}, s_{V_{0+}}^{0\nu^-}, s_{V}^{0\nu^-}, s_{A_{1+}}^{0\nu^-}, s_A^{0\nu^-}$ , and  $s^{0\nu^-}$  in  ${}^{76}\text{Ge}$ , using the parametrization P2.

From this figure it is clear note that the densities  $\mathcal{S}_{00}^{\{-2\}}$  and  $\mathcal{S}_V^{0\nu^-} \cong \mathcal{S}_{V_{0+}}^{0\nu^-}$  behave similarly to each other, as do  $\mathcal{S}_{10}^{\{-2\}}$  and  $\mathcal{S}_A^{0\nu^-} \cong \mathcal{S}_{A_{1+}}^{0\nu^-}$ . They are concentrated, respectively, at  $\sim 21$  MeV, and at  $\sim 13$  MeV, where the corresponding DCE resonances, *i.e.*, the Double Isobaric Analog State (DIAS), and the Double Monopole Gamow-Teller Resonance (DMGTR), are localized.

Our DCETDA result for DIAS energy agrees well with the analytical estimate by Roca-Maza, Sagawa and Colò [65] given by

$$\mathcal{E}_{DIAS} = 2\mathcal{E}_{IAS} + \Delta\mathcal{E}_{Coul}, \quad (46)$$

where  $\mathcal{E}_{IAS}$  is the energy of the isobaric analog state (IAS), defined as

$$\mathcal{E}_{IAS} = \mathcal{E}_{Coul}(Z, A) - \mathcal{E}_{Coul}(Z, A - 1). \quad (47)$$

The Coulomb energies are taken from [64, (2-19)], *i.e.*,

$$\mathcal{E}_{Coul}(Z, A) = 0.70 \frac{Z^2}{A^{1/3}} [1 - 0.76Z^{-2/3}] \text{ MeV}, \quad (48)$$

while from [65, (19)]

$$\Delta\mathcal{E}_{Coul} \cong \frac{3}{2} A^{-1/3} \text{ MeV}. \quad (49)$$

From Eq. (46) we now obtain  $\mathcal{E}_{DIAS} = 2 \times 10.21 + 0.35 \text{ MeV} = 20.77 \text{ MeV}$ , which agrees perfectly with our nuclear model calculations, given in Fig. 3 by the peak energy of  $\mathcal{S}_{00}^{\{-2\}}$ .

As shown in the same figure the DCER quadrupole strength  $\mathcal{S}_{12}^{\{-2\}}$ , and its double quadrupole Gamow-Teller resonance (DQGTR) at  $\sim 14$  MeV. As mentioned above, this resonance is not related to the Majorana mass. However, the comparison between calculations and experimental data are important to test the nuclear models.

The total density distribution  $\mathcal{S}^{0\nu^-}$  is the envelope of  $\mathcal{S}_V^{0\nu^-}$ , and  $\mathcal{S}_A^{0\nu^-}$ , including also the pseudoscalar and weak magnetism contributions. Very similar spectra are obtained when the parameterization P1 is used, with the main differences being: (i) the axial vector strength now peaks at  $\sim 15$  MeV, and (ii) the insertion plot is modified somewhat, as indicated in Table IV.

Needless to say, only the NMEs that are within the  $Q$ -value window (shown in the inset of Figure 3), are significant to the neutrino mass. It is relevant to note in this insert the similarity of  $s_{10}^{\{-2\}}$  with  $s_{A_{1+}}^{0\nu^-}$  and its difference with  $s^{0\nu^-}$ . Of course, the same issue can be seen in Table III.

However, the entire reaction spectrum ( $\mathcal{S}_{00}^{\{-2\}} + \mathcal{S}_{10}^{\{-2\}}$ ) can, in principle, be measured, and especially in

the region of DIAS, and DMGTR resonances, which are well separated from each other. It would then be worthwhile to perform such a measurement, and compare the resulting data with theoretical predictions, in line with what was done in Ref. [27] for the two GT spectra  $\mathcal{S}_{10}^{\{\mp 1\}}$  in  $^{48}\text{Sc}$ , and in Ref. [66] for the GT spectrum  $\mathcal{S}_{10}^{\{-1\}}$  in  $^{132}\text{Sb}$ . Agreement between such measurements with the calculations shown in Figure 3 them would test our nuclear structure model, as well as that the predictions about the NMEs make sense.

## F. Relationships between calculations and reaction data

The question posed here is whether the DCE transition strengths  $\mathcal{S}_{J\mathcal{J}}^{\{\pm 2\}}$  are experimentally accessible, in the same way as the SCE strengths  $\mathcal{S}_{10}^{\{\pm 1\}}$  [27, 66] are?

It should be recalled here that in the SCE case it is possible to study GT transitions via light-ion-induced reactions, such as (n,p), (p,n), ( $^3\text{He,t}$ ), and (t, $^3\text{He}$ ), thanks to the proportionality relationship between the zero angular momentum transfer cross section,  $\sigma$  (at a forward angle) and the corresponding GT strength  $s_1^{\{-1\}}$  (see [27, Eq. (3)], and [66, Eq. (1)]). Namely,

$$\sigma_{SCE-GT} \sim \mathcal{S}_1^{\{-1\}}, \quad (50)$$

where the strength density  $\mathcal{S}_1^{\{-1\}}$  in the odd-odd nucleus is defined in the same way as  $\mathcal{S}_{J\mathcal{J}}^{\{-2\}}$  in Eq. (12) for the final nucleus, with  $s_J^{\{\mp 1\}}(J_i)$  instead of  $s_{J\mathcal{J}}^{\{\mp 2\}}(\mathcal{J}_f)$ .

In the DCE case happens something similar in the ( $\pi^+$ ,  $\pi^-$ ) reactions, but only with Fermi transitions, for which

$$\sigma_{DCE-F} \sim S_{00}^{\{2\}} \cong S_{00}^{\{-2\}}, \quad (51)$$

as demonstrated in [62, Fig. 1] (see also [63]). Moreover, in the spectrum  $\mathcal{S}_{00}(\mathcal{E})$ , the DIAS resonance is clearly perceived at the energy  $\mathcal{E}_{DIAS}$ , given by Eq. (46), as can be seen in [69, Fig. 2]. Moreover, the Fig. 3 shows that the DIAS is a rather narrow resonance in the Fermi spectra  $\mathcal{S}_{00}(\mathcal{E})$ , suggesting that near its maximum at  $\mathcal{E}_{DIAS}$ , it behaves like

$$\sigma_{DCE-F} \sim \mathcal{S}_{00}^{\{-2\}}(\mathcal{E}). \quad (52)$$

The pion, however, interacts weakly with states involving the spin degree of freedom, and therefore states such as DMGTR and DQGTR are not observed in ( $\pi^+$ ,  $\pi^-$ ) reactions.

As mentioned above, heavy ion DCE reactions are being carried out using light ions such as  $^{18}\text{O}$ . It is hoped to learn something about the magnitude of the  $0\nu\beta\beta$  NMEs by measuring the  $M_{00}$ , and  $M_{10}$ , whose weak analogs  $M_{V_{0+}}^{0\nu}$ , and  $M_{A_{1+}}^{0\nu}$  are the major contributor to them, as seen in Table III, and discussed in detail above.

The difficulty is due these heavy ion DCE reactions are much more complicated than those of ( $\pi^+$ ,  $\pi^-$ ), especially since they probe the NMEs of the projectile and the target at the same time, requiring additional theoretical efforts to disentangle the two types of contributions [8, 61, 71]. In this scenario, the Gawow-Teller cross section cannot be expressed in the form of the Fermi cross section, given by Eq. (52).

Based on a previous work of Bertulani [72], Santopinto *et al.*[15] have recently reported that, for the ground-state target nuclei the DCE differential cross section within the low-momentum-transfer limit can be factored into: i) a reaction part, which is computed by means of the eikonal approximation, and ii) the nuclear part

$$\mathcal{N} = \left| \frac{M_{00}^P M_{00}^T}{\bar{E}_0^P + \bar{E}_0^T} + \frac{M_{10}^P M_{10}^T}{\bar{E}_1^P + \bar{E}_1^T} \right|^2, \quad (53)$$

where  $P$  and  $T$  stand for projectile and target nuclei respectively, and

$$\bar{E}_J = \frac{\sum_i s_J^{\{-1\}}(J_i)(E_{J_i}^{\{-1\}} - E_{0+}^{\{0\}})}{S_J^{\{-1\}}} \quad (54)$$

are the averaged energies of the intermediate nucleus (see (1)). The purpose is to put an upper limit on  $M_{10}^T$ , which will correspond to an upper limit on  $M^{0\nu}$  for  $\beta\beta$ -decaying nuclei. Something similar has been done previously by Cappuzzello *et al.*[71] for the reaction  $^{40}\text{Ca}(^{18}\text{O}, ^{18}\text{Ne})^{40}\text{Ar}$ , in which the  $\beta\beta$ -decay does not occur.

All NMEs and energies in (53) can be calculated straightforward in the DCEQTDA, and we only need the experimental values of  $\mathcal{N}$  to make the comparison with the data. This would be the first step toward the calibration of  $M^{0\nu}$  by heavy ion reaction experiments.

Finally, it should be noted that only at low momentum transfer are the NMEs in heavy-ion reactions of the form of Eq. (33), where only the intermediate  $J^\pi = 0^+, 1^+$  states contribute, as in  $2\nu\beta\beta$ -decay. In fact, as pointed out in Ref. [61], the transition amplitude requires in the general case the inclusion of all multipole terms with  $J^\pi = 0^\pm, 1^\pm, \dots, 10^\pm$ , since the momentum transferred is of the order of  $q \geq 400$  MeV/c as in the  $0\nu\beta\beta$  decay, where  $q \sim 100$  MeV/c [76].

## IV. SUMMARY AND FINAL REMARKS

The central objective of the present work was to complete the formulation of the DCEQTDA, which was proposed some time ago [39], and developed in detail for application to the  $2\nu\beta\beta$ -decay [26]. Here, in Section II, we extend it to the  $0\nu\beta\beta$ -decay. In Section II we also present, as a byproduct, the formulas for the  $Q$ -values for  $\beta\beta$ -decay and  $ee$ -capture, and for low momentum transfer reaction NMEs.

In Section III we apply the whole DCEQTDA formalism to the  $^{76}\text{Ge}$  decay, and to the  $ee$ -capture in  $^{124}\text{Xe}$ .

First, in Section III B we study all the DCE observables that have been measured so far, both the static ones (excitation energies in the final nuclei, and the  $Q_{\beta\beta^-}$  and  $Q_{ee}$  values), and the dynamic ones which are the  $\tau_{2\nu}$  half-lives of all  $0^+$  and  $2^+$  states that lie within the windows of  $Q$  values, obtaining good agreement with the experimental data for all of them.

After thus ensuring the reasonableness of the DCE-QTDA, we used in Section III C that nuclear model to study the  $0\nu\beta\beta$ -decay and  $0\nu ee$ -captures in the same nuclei. We start in Section III C 1 with the analysis of the genesis of the  $0\nu\beta\beta$ -decay to the ground state in  $^{76}\text{Se}$ , comparing it with the results of the  $pn$ -QRPA. We find that these two nuclear models are physically very different and that the main reason is the absence of the Pauli Principle in the description of  $^{76}\text{Se}$  in the second model. In Section III C 2 we make a brief comparison of our results for the  $0\nu\beta\beta$  NMEs, with those obtained in previous studies, observing that in DCEQTDA they turn out to be significantly lower than in most of the other nuclear models. Finally, in Section III C 3 we point out that it is not correct to associate the reaction NMEs  $M_{00}$  and  $M_{10}$  with the  $0\nu\beta\beta$  NMEs  $M_V^{0\nu}$ , and  $M_A^{0\nu}$ , as is often done.

In Section III D we have calculated total strengths  $S_{JJ}^{\{\mp 2\}}$  in  $^{76}\text{Ge}$ , and  $^{124}\text{Xe}$ . So far, this had been done only for light nuclei up to  $^{48}\text{Ca}$  [4, 13]. To calibrate the  $0\nu\beta\beta$  NMEs we have also done so for the total strengths  $S_{V,A}^{0\nu\mp}$ , which has never been done before. We conclude that the fractions of  $S_{JJ}^{\{\mp 2\}}$  and  $S_{V,A}^{0\nu\mp}$  are of the order of  $10^{-4} - 10^{-3}$  in  $0\nu\beta\beta$ -decays and still smaller in  $0\nu ee$ -capture processes.

The comparison made in Table IV between reaction and  $0\nu\beta\beta$  NMEs is extended in Section III E by exposing in Fig. 3 the full spectral densities  $\mathcal{S}_{JJ}^{\{-2\}}$ , and  $\mathcal{S}_{V,A}^{0\nu-}$ , which also include the giant DCE resonances. The fact that they turned out to be of the same order came as a surprise, as we have found no physical reason to justify it.

We have advanced to the energy region where giant DCE resonances should be found, aware that  $\beta\beta$ -decays cannot occur there. However, experimental verification of our prediction, however, would reinforce confidence in the theoretical comparison made.

Although the main motive of this work has been the study of  $\beta\beta$ -decays, and in particular of the  $0\nu$ -mode, in Section III F we also briefly discuss nuclear reaction experiments, which are related to this decay mode.

We demonstrate that theoretical methods are at hand, ready to describe the DCE reaction data at low momentum transfer that will be available in the near future.

The present nuclear structure model contains the same free parameters as the  $pn$ -QRPA model, and is specially designed to describe double charge exchange processes. As such, in addition to incorporating the pairing correlations it has the following features:

1) It contains four-quasiparticle excitations and the Pauli principle, which play a crucial role,

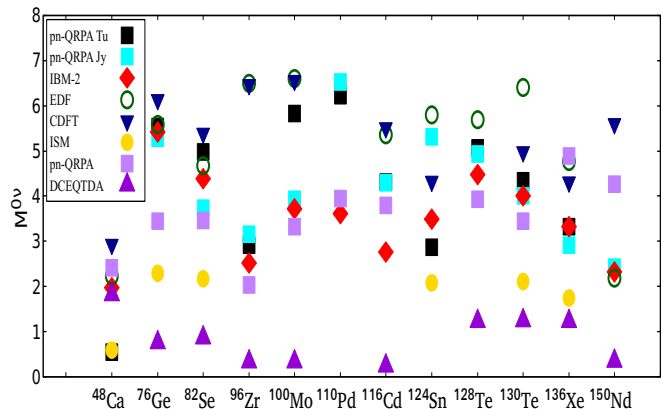


FIG. 4: (Color online) Comparison of calculated NMEs  $M^{0\nu-}(0_1^+) \equiv M^{0\nu}$ , within several nuclear structure models: i)  $pn$ -QRPA by Tübingen group (QRPA Tu) [55] ( $g_A = 1.27$ ), ii)  $pn$ -QRPA by Jyväskylä group (QRPA Jy) [56] ( $g_A = 1.26$ ), iii) Interacting Boson Model (IBM-2) [78] ( $g_A = 1.269$ ), iv) Energy Density Functional Method (EDF) [79] ( $g_A = 1.25$ ), v) Covariant Density Functional Theory (CDFT) [80, 81] ( $g_A = 1.254$ ), vi) Interacting Shell Model (ISM) [77] ( $g_A = 1.25$ ), and finally are shown the present  $pn$ -QRPA and DCEQTDA ( $g_A = 1.27$ ) results. All results are normalized to  $g_A^2$ . This figure is similar to [81, Fig. 7], [82, Fig. 5], [83, Fig. 4], and [84, Fig. 1].

2) It allows working with a single-particle space large enough for the DCE sum rules to be satisfied; and

3) it jointly describes the  $\beta\beta$ -decays and DCERs to all  $0^+$  and  $2^+$  final states, as well as their  $Q$ -values, energies, resonances and sum rules.

We believe that these three aspects are indispensable for a reliable assessment of  $0\nu\beta\beta$  NMEs. The commonly used  $pn$ -QRPA model, being limited to the description of ground-state NMEs, does not meet these conditions. The model that comes closest to these requirements is the shell model [4].

Last but not least, in Fig. 4 we compare the present  $pn$ -QRPA and DCEQTDA calculations for several ground state  $0\nu\beta\beta$  NMEs, performed with the same residual interaction and identical nuclear model parameters. We also show the results of  $pn$ -QRPA calculations performed with more realistic residual interactions, such as induced by the exchange of a G boson, as well as the results of calculations of other nuclear models. It can be inferred that, except for  $^{48}\text{Ca}$ , the new DCEQTDA model produces results that are definitely smaller than the other nuclear structure models; going (for  $g_A = 1.27$ ) from 0.12 in  $^{116}\text{Cd}$  to 1.7 in  $^{48}\text{Ca}$ . We attribute this difference mainly to the effect of the Pauli Principle. The calculation most similar to our DCEQTDA is that of the ISM [77] ( $g_A = 1.25$ ), although it was done in a small single-particle space. A more complete calculation of these NMEs will be carried out by analyzing all nuclei in which double beta and double electron capture processes occur.

### Acknowledgments

We sincerely thank Wayne Seale for careful and enlightening reading of the manuscript. This work was financed in part by the Coordenação de Aperfeiçoamento de Pessoal de Nível Superior Brasil Fi-

nance Code 001. A.R.S. acknowledges the financial support of Fundação de Amparo à Pesquisa do Estado da Bahia (T.O. PIE0013/2016) and the partial support of UESC (PROPP 00220.1300.1832 and SEI 073.6766.2020.0010299-61). V. dos S. F. acknowledges the financial support of UESC-PROBOL program.

- 
- [1] C. Brase, J. Menéndez, E. A. Coello Pérez, and A. Schwenk, arXiv:2108.11805v1 [nucl-th].
- [2] D. C. Zheng, L. Zamick, and N. Auerbach, *Phys. Rev. C* **40**, 936 (1989).
- [3] N. Auerbach, L. Zamick, D.C. Zheng, *Annals of Phys.* **192**, 77 (1989).
- [4] N. Auerbach, and Bui MinhLoc, *Phys. Rev. C* **98**, 064301 (2018).
- [5] N. Auerbach, in *Journal of Physics: Conference Series* (IOP Publishing, 2018), vol. 1023, p. 012032.
- [6] M. Agostini *et al.* (GERDA Collaboration), *Phys. Rev. Lett.* **125**, 252502 (2020).
- [7] I. J. Arnquist *et al.* (Majorana Collaboration), *Phys. Rev. C* **103**, 015501 (2021).
- [8] H. Lenske, F. Cappuzzello, M. Cavallaro, and M. Colonna, *Prog. Part. Nucl. Phys.* **109**, 103716 (2019).
- [9] M. Cavallaro, L. Acosta, P. Adsley, C. Agodi, C. Altana *et al.*, *J. Phys. Conf. Ser.* **1610**, 012004 (2020).
- [10] P. Finocchiaro *et al.*, for the Numen Collaboration, *Universe* **6** (9), 129 (2020).
- [11] C. Agodi, F. Cappuzzello, L. Acosta, C. Altana, P. Amador-Valenzuela *et al.*, *JPS Conf. Proc.* **32**, 010045 (2020).
- [12] F. Cappuzzello, M. Cavallaro, *Universe* **6** (11), 217 (2020).
- [13] N. Shimizu, J. Menéndez, and K. Yako, *Phys. Rev. Lett.* **120**, 142502 (2018).
- [14] J. Menéndez, N. Shimizu, and K. Yako, *J. Phys. Conf. Ser.* **1056**, 012037 (2018).
- [15] E. Santopinto, H. García-Tecocoatzi, R. I. Magaña Vsevolodovna, and J. Ferretti, (NUMEN Collaboration), *Phys. Rev. C* **98**, 061601(R) (2018).
- [16] E. Santopinto, J. Ferretti, H. García-Tecocoatzi, R.I. Magana Vsevolodovna, within the NUMEN project, *J. Phys. Conf. Ser.* **1610**, 012013 (2020).
- [17] E. Aprile *et al.*, *Nature* **568** (2019).
- [18] K. Hiraide *et al.* (XMASS Collaboration.), in *J. Phys. Conf. Ser.* **1342** (IOP Publishing), 1342, 012027 (2020).
- [19] K. Ikeda, S. Fujii, and J. I. Fujita, *Phys. Lett.* **3**, 271 (1963).
- [20] P. Vogel, M. Ericson, and J. D. Vergados, *Phys. Lett. B* **212**, 259 (1988).
- [21] K. Muto, *Phys. Lett. B* **277**, 13 (1992).
- [22] C. Barbero, F. Krmpotić, and D. Tadić, *Nucl. Phys. A* **628**, 170 (1998).
- [23] C. Barbero, F. Krmpotić, A. Mariano, and D. Tadić, *Nucl. Phys. A* **650**, 485 (1999).
- [24] T. Tomoda, *Phys. Lett. B* **474**, 245 (2000).
- [25] R. A. Sen'kov and M. Horoi, *Phys. Rev. C* **88**, 064312 (2013).
- [26] V. dos S. Ferreira, F. Krmpotić, C.A. Barbero, A.R. Samana, *Phys. Rev. C* **96**, 044322 (2017).
- [27] K. Yako, *Phys. Rev. Lett.* **103**, 012503 (2009).
- [28] J. A. Halbleib and R. A. Sorensen, *Nucl. Phys. A* **98**, 542 (1967).
- [29] P. Vogel and M. R. Zirnbauer, *Phys. Rev. Lett* **57**, 3148 (1986).
- [30] O. Civitarese, A. Faessler and T. Tomoda, *Phys. Lett. B* **194**, 11 (1987).
- [31] T. Tomoda and A. Faessler, *Phys. Lett. B* **199**, 475 (1987).
- [32] J. Engel, P. Vogel and M. R. Zirnbauer, *Phys. Rev. C* **37**, 731 (1988).
- [33] J. Hirsch and F. Krmpotić, *Phys. Rev. C* **41**, 792 (1990).
- [34] J. Hirsch and F. Krmpotić, *Phys. Lett. B* **246**, 5 (1990).
- [35] J. Hirsch, E. Bauer and F. Krmpotić, *Nucl. Phys. A* **516**, 304 (1990).
- [36] A. Staudt, K. Muto, H.V. Klapdor-Kleingrothaus, *Europhys. Lett.* **13**, 31 (1990).
- [37] F. Krmpotić, J. Hirsch and H. Dias, *Nucl. Phys. A* **542**, 85 (1992).
- [38] F. Krmpotić, and S. Shelly Sharma, *Nucl. Phys. A* **572**, 329 (1994).
- [39] F. Krmpotić, *Fizika B* **14**, 139 (2005).
- [40] V. dos S. Ferreira, A.R. Samana, F. Krmpotić, and M. Chiapparini, *Phys. Rev. C* **101**, 044314 (2020).
- [41] D. Gambacurta and M. Grasso, *Eur. Phys. J. A* **52**, 1 (2016).
- [42] F. Šimkovic, G. Pantis, J. D. Vergados and A. Faessler, *Phys. Rev. C* **60**, 055502 (1999).
- [43] J. M. Yao, L. S. Song, K. Hagino, P. Ring, and J. Meng, *Phys. Rev. C* **91**, 024316 (2015).
- [44] J. Beringer *et al.* (Particle Data Group), *Phys. Rev. D* **86**, 010001 (2012).
- [45] J. D. Walecka, *Theoretical nuclear and subnuclear physics* (World Scientific Publishing Company, 2004).
- [46] M. Mirea, T. Pahomi, and S. Stoica, *Rom. Rep. in Phys.* **67**, 872 (2015).
- [47] J. Suhonen, O. Civitarese, *Phys. Rep.* **300**, 123 (1998).
- [48] M. Aunola, J. Suhonen, *Nuc. Phys. A* **602**, 133 (1996).
- [49] B. Pritychenko, National Nuclear Data Center, <http://www.nndc.bnl.gov/> (2011).
- [50] P. Pirinen and J. Suhonen, *Phys. Rev. C* **91**, 054309 (2015).
- [51] E. Coello Pérez, J. Menéndez, and A. Schwenk, *Phys. Lett. B* **797**, 134885 (2019).
- [52] F. Krmpotić, M. N. Rao, O. Sala and A. Szanto de Toledo, *Phys. Rev. C* **16** 438 (1977).
- [53] A. Barabash, *Universe* **6**(10), 159 (2020).
- [54] J. Kotila, and F. Iachello, *Phys. Rev. C* **87**, 024313 (2013).
- [55] F. Šimkovic, V. Rodin, A. Faessler, and P. Vogel, *Phys. Rev. C* **87**, 045501 (2013).
- [56] J. Hyvärinen and J. Suhonen, *Phys. Rev. C* **91**, 024613 (2015).
- [57] A. Belley, C. G. Payne, S. R. Stroberg, T. Miyagi, and

- J. D. Holt, Phys. Rev. Lett. **126**, 042502 (2021).
- [58] J. Barea, J. Kotila, and F. Iachello, Phys. Rev. C **87**, 057301 (2013).
- [59] J. Suhonen, From Nucleons to Nucleus: Concepts of Microscopic Nuclear Theory (Springer, Berlin, 2007).
- [60] D.L. Fang and A. Faessler, Phys. Rev. C **103**, 045501(2021).
- [61] J. I. Bellone, M. Colonna, J. A. Lay, and H. Lenske ( NUMEN Collaboration), Phys. Lett. B **807**, 135528 (2020).
- [62] M. Kaletka, K. K. Seth, A. Saha et al., Phys. Lett. B **199**, 336 (1987).
- [63] N. Auerbach, W.R. Gibbs, E. Piasezky, Phys. Rev. Lett. **59**, 1076 (1987).
- [64] A. Bohr and B.R. Mottelson, *Nuclear Structure, Vol. 1* (W. A. Benjamin, New York, Amsterdam, 78, 1969).
- [65] X. Roca-Maza, H. Sagawa, G. Colo, Phys. Rev. C **101**, 014320 (2020).
- [66] J. Yasuda, M. Sasano, R.G.T. Zegers, H. Baba, D. Bazin et al. Phys. Rev. Lett. **121** 13, 132501 (2018).
- [67] J. Kostensalo, J. Suhonen, K. Zuber, Phys. Lett. B **831**, 137170 (2022).
- [68] M. Aunola, J. Suhonen, Nucl. Phys. A **602**, 133 (1996).
- [69] N. Auerbach, Ann. Phys. **197**, 376395 (1990).
- [70] M. Doi, Prog. Theor. Phys. **89**, 139 (1993).
- [71] F. Cappuzzello et al., Eur. Phys. J. A **51**, 145 (2015).
- [72] C. A. Bertulani, Nucl. Phys. A **554**, 493 (1993).
- [73] F. Šimkovic, A. Faessler, V. Rodin, P. Vogel, J. Engel, Phys. Rev. C **77**, 045503 (2008).
- [74] R. A. Sen'kov and M. Horoi, Phys. Rev. C **90**, 051301(R) (2014),
- [75] H. Sagawa and T. Uesaka, Phys. Rev. C **94**, 064325 (2016).
- [76] T. Tomoda, Rep. Prog. Phys. **54**, 53 (1991).
- [77] J. Menéndez, A. Poves, E. Caurier and F. Nowacki, D, Nucl. Phys. A **818**, 139 (2009).
- [78] J. Barea, J. Kotila and F. Iachello, Phys. Rev. C **87**, 014315 (2013).
- [79] N. L. Vaquero, T. R. Rodríguez and J. L. Egidio, Phys. Rev. Lett. **111**, 142501 (2013).
- [80] L.S. Song, J.M. Yao, P. Ring, J. Meng, Phys. Rev. C **90**, 054309 (2014).
- [81] J. M. Yao, L. S. Song, K. Hagino, P. Ring, and J. Meng, Phys. Rev. C **91**, 024316 (2015).
- [82] J. Engel and J. Menéndez, Rept. Prog. Phys. **80**, 046301 (2017), and arXiv:1610.06548.
- [83] J.J. Gómez-Cadenas, and J. Martín-Albo, PoS **GSSI14**, 004 (2015).
- [84] J. Menéndez, arXiv:1605.05059.